Electronic Supplementary Material (ESI) for Physical Chemistry Chemical Physics.

Supplementary information for 'Two-gap-like anisotropic superconductivity in bulk boron kagome lattice'

Shuming Zeng,[1] Geng Li,[2,3,*] and Yinchang Zhao[4,†]

[1] *College of Physics Science and Technology, Yangzhou University, Jiangsu 225009, P. R. China.*

[2] *School of Materials Science and Engineering, National Institute for Advanced Materials, Nankai University, Tongyan Road 38, Tianjin 300350, China.*

[3] *National Supercomputer Center in Tianjin, Tianjin 300457, China.*

[4] *Department of Physics, Yantai University, Shandong 264005, P. R. China*

(Dated: September 24, 2023)

S1. Detailed structural parameters for eight considered boron structures

The atomic structures for eight considered boron allotropes in the main text are plotted in Fig. S1, where the black line in each panel denotes the primitive cell. The detailed structural parameters of these boron allotropes are listed in Table. I. One can observe that there are 12, 105, 2, 6, 10, 12, 1, and 2 atoms in the primitive cells of α bulk boron, β bulk boron, δ_6 buckled borophene, bulk boron kagome lattice, (5, 0) boron nanotube, (6, 0) boron nanotube, δ_6 flat borophene, and δ_3 borophene, respectively.

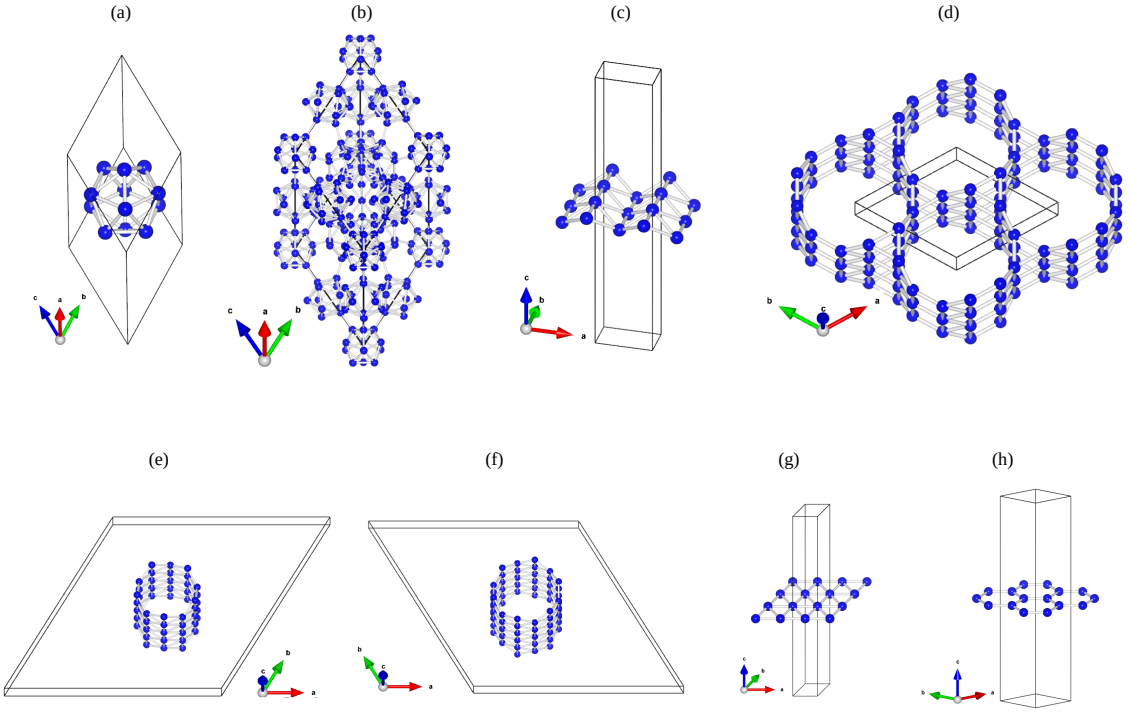

FIG. S1. Atomic structures for eight considered boron allotropes: (a) α bulk boron, (b) β bulk boron, (c) δ_6 buckled borophene, (d) bulk boron kagome lattice, (e) (5, 0) boron nanotube, (f) (6, 0) boron nanotube, (g) δ_6 flat borophene, and (f) δ_3 borophene.

TABLE I: Structural parameters for α bulk boron, β bulk boron, δ_6 buckled borophene, bulk boron kagome lattice, (5, 0) boron nanotube, (6, 0) boron nanotube, δ_6 flat borophene, and δ_3 borophene.

	a (Å)	b (Å)	c (Å)	α (°)	β (°)	γ (°)	Atomic positions
α bulk	5.05	5.05	5.05	58.03	58.03	58.03	B_1 (0.15406, 0.51032, 0.51032)
							B_2 (0.51032, 0.15406, 0.51032)
							B_3 (0.51032, 0.51032, 0.15406)
							B_4 (0.48968, 0.48968, 0.84594)
							B_5 (0.84594, 0.48968, 0.48968)
							B_6 (0.48968, 0.84594, 0.48968)
							B_7 (0.13048, 0.72111, 0.72111)
							B_8 (0.72111, 0.13048, 0.72111)
							B_9 (0.72111, 0.72111, 0.13048)
							B_{10} (0.27889, 0.27889, 0.86952)
							B_{11} (0.86952, 0.27889, 0.27889)
							B_{12} (0.27889, 0.86952, 0.27889)
β bulk	10.12	10.12	10.12	65.30	65.30	65.30	B_1 (0.00281, 0.16347, 0.00281)
							B_2 (0.00281, 0.00281, 0.16347)
							B_3 (0.16347, 0.00281, 0.00281)
							B_4 (0.83653, 0.99719, 0.99719)
							B_5 (0.99719, 0.83653, 0.99719)
							B_6 (0.99719, 0.99719, 0.83653)
							B_7 (0.09970, 0.84118, 0.09970)
							B_8 (0.09970, 0.09970, 0.84118)
							B_9 (0.84118, 0.09970, 0.09970)
							B_{10} (0.15882, 0.90030, 0.90030)
							B_{11} (0.90030, 0.15882, 0.90030)
							B_{12} (0.90030, 0.90030, 0.15882)
							B_{13} (0.99546, 0.66405, 0.99546)

a (Å)	b (Å)	c (Å)	α (°)	β (°)	γ (°)	Atomic positions
						B_{14} (0.99546, 0.99546, 0.66405)
						B_{15} (0.66405, 0.99546, 0.99546)
						B_{16} (0.33595, 0.00454, 0.00454)
						B_{17} (0.00454, 0.33595, 0.00454)
						B_{18} (0.00454, 0.00454, 0.33595)
						B_{19} (0.10409, 0.49032, 0.10409)
						B_{20} (0.10409, 0.10409, 0.49032)
						B_{21} (0.49032, 0.10409, 0.10409)
						B_{22} (0.50968, 0.89591, 0.89591)
						B_{23} (0.89591, 0.50968, 0.89591)
						B_{24} (0.89591, 0.89591, 0.50968)
						B_{25} (0.34899, 0.00386, 0.17461)
						B_{26} (0.17461, 0.34899, 0.00386)
						B_{27} (0.00386, 0.17461, 0.34899)
						B_{28} (0.99614, 0.65101, 0.82539)
						B_{29} (0.82539, 0.99614, 0.65101)
						B_{30} (0.65101, 0.82539, 0.99614)
						B_{31} (0.65101, 0.99614, 0.82539)
						B_{32} (0.82539, 0.65101, 0.99614)
						B_{33} (0.99614, 0.82539, 0.65101)
						B_{34} (0.00386, 0.34899, 0.17461)
						B_{35} (0.17461, 0.00386, 0.34899)
						B_{36} (0.34899, 0.17461, 0.00386)
						B_{37} (0.55093, 0.89514, 0.16593)
						B_{38} (0.16593, 0.55093, 0.89514)
						B_{39} (0.89514, 0.16593, 0.55093)
						B_{40} (0.10487, 0.44908, 0.83407)
						B_{41} (0.83407, 0.10487, 0.44908)

a (Å)	b (Å)	c (Å)	α (°)	β (°)	γ (°)	Atomic positions
						B_{42} (0.44908, 0.83407, 0.10487)
						B_{43} (0.44908, 0.10487, 0.83407)
						B_{44} (0.83407, 0.44908, 0.10487)
						B_{45} (0.10487, 0.83407, 0.44908)
						B_{46} (0.89514, 0.55093, 0.16593)
						B_{47} (0.16593, 0.89514, 0.55093)
						B_{48} (0.55093, 0.16593, 0.89514)
						B_{49} (0.19896, 0.68660, 0.19896)
						B_{50} (0.19896, 0.19896, 0.68660)
						B_{51} (0.68660, 0.19896, 0.19896)
						B_{52} (0.31340, 0.80104, 0.80104)
						B_{53} (0.80104, 0.31340, 0.80104)
						B_{54} (0.80104, 0.80104, 0.3134)
						B_{55} (0.68402, 0.20023, 0.37561)
						B_{56} (0.37561, 0.68402, 0.20023)
						B_{57} (0.20023, 0.37561, 0.68402)
						B_{58} (0.79977, 0.31598, 0.62439)
						B_{59} (0.62439, 0.79977, 0.31598)
						B_{60} (0.31598, 0.62439, 0.79977)
						B_{61} (0.31598, 0.79977, 0.62439)
						B_{62} (0.62439, 0.31598, 0.79977)
						B_{63} (0.79977, 0.62439, 0.31598)
						B_{64} (0.20023, 0.68402, 0.37561)
						B_{65} (0.37561, 0.20023, 0.68402)
						B_{66} (0.68402, 0.37561, 0.20023)
						B_{67} (0.58021, 0.09603, 0.36361)
						B_{68} (0.36361, 0.58021, 0.09603)
						B_{69} (0.09603, 0.36361, 0.58021)

a (Å)	b (Å)	c (Å)	α (°)	β (°)	γ (°)	Atomic positions
						B_{70} (0.90397, 0.41979, 0.63639)
						B_{71} (0.63639, 0.90397, 0.41979)
						B_{72} (0.41979, 0.63639, 0.90397)
						B_{73} (0.41979, 0.90397, 0.63639)
						B_{74} (0.63639, 0.41979, 0.90397)
						B_{75} (0.90397, 0.63639, 0.41979)
						B_{76} (0.09603, 0.58021, 0.36361)
						B_{77} (0.36361, 0.09603, 0.58021)
						B_{78} (0.58021, 0.36361, 0.09603)
						B_{79} (0.19920, 0.50587, 0.19920)
						B_{80} (0.19920, 0.19920, 0.50587)
						B_{81} (0.50587, 0.19920, 0.19920)
						B_{82} (0.49413, 0.80080, 0.80080)
						B_{83} (0.80080, 0.49413, 0.80080)
						B_{84} (0.80080, 0.80080, 0.49413)
						B_{85} (0.38445, 0.56820, 0.38445)
						B_{86} (0.38445, 0.38445, 0.56820)
						B_{87} (0.56820, 0.38445, 0.38445)
						B_{88} (0.43180, 0.61555, 0.61555)
						B_{89} (0.61555, 0.43180, 0.61555)
						B_{90} (0.61555, 0.61555, 0.43180)
						B_{91} (0.48929, 0.22118, 0.48929)
						B_{92} (0.48929, 0.48929, 0.22118)
						B_{93} (0.22118, 0.48929, 0.48929)
						B_{94} (0.77882, 0.51072, 0.51072)
						B_{95} (0.51072, 0.77882, 0.51072)
						B_{96} (0.51072, 0.51072, 0.77882)
						B_{97} (0.38150, 0.21358, 0.38150)

	a (Å)	b (Å)	c (Å)	α (°)	β (°)	γ (°)	Atomic positions
							B_{98} (0.38150, 0.38150, 0.21358)
							B_{99} (0.21358, 0.38150, 0.38150)
							B_{100} (0.78642, 0.61850, 0.61850)
							B_{101} (0.61850, 0.78642, 0.61850)
							B_{102} (0.61850, 0.61850, 0.78642)
							B_{103} (0.38481, 0.38481, 0.38481)
							B_{104} (0.61519, 0.61519, 0.61519)
							B_{105} (0.50000, 0.50000, 0.50000)
δ_6 buckled sheet	2.87	1.62	14.87	90.00	90.00	90.00	B_1 (0.00000, 0.00000, 0.52987)
							B_2 (0.50000, 0.50000, 0.47013)
bulk kagome	5.98	5.98	1.89	90.00	90.00	120.0	B_1 (0.56862, 0.13724, 0.25000)
							B_2 (0.56862, 0.43138, 0.25000)
							B_3 (0.86276, 0.43138, 0.25000)
							B_4 (0.13724, 0.56862, 0.75000)
							B_5 (0.43138, 0.56862, 0.75000)
							B_6 (0.43138, 0.86276, 0.75000)
(5,0) nanotube	19.30	19.30	1.62	90.00	90.00	60.00	B_1 (0.53387, 0.62102, 0.75000)
							B_2 (0.43376, 0.66197, 0.25000)
							B_3 (0.35899, 0.64101, 0.75000)
							B_4 (0.33803, 0.56624, 0.25000)
							B_5 (0.37898, 0.46613, 0.75000)
							B_6 (0.46613, 0.37898, 0.25000)
							B_7 (0.56624, 0.33803, 0.75000)
							B_8 (0.64101, 0.35899, 0.25000)
							B_9 (0.66197, 0.43376, 0.75000)
							B_{10} (0.62102, 0.53387, 0.25000)
(6,0) nanotube	20.34	20.34	1.62	90.00	90.00	120.0	B_1 (0.63102, 0.67897, 0.00000)
							B_2 (0.67897, 0.63102, 0.50000)

	a (Å)	b (Å)	c (Å)	α (°)	β (°)	γ (°)	Atomic positions
							B_3 (0.45204, 0.63102, 0.00000)
							B_4 (0.54796, 0.67897, 0.50000)
							B_5 (0.32103, 0.45204, 0.00000)
							B_6 (0.36898, 0.54796, 0.50000)
							B_7 (0.36898, 0.32103, 0.00000)
							B_8 (0.32103, 0.36898, 0.50000)
							B_9 (0.54796, 0.36898, 0.00000)
							B_{10} (0.45204, 0.32103, 0.50000)
							B_{11} (0.67897, 0.54796, 0.00000)
							B_{12} (0.63102, 0.45204, 0.50000)
δ_6 flat sheet	1.71	1.71	15.15	90.00	90.00	60.00	B_1 (0.00000, 0.00000, 0.50000)
δ_3 sheet	2.92	2.92	15.58	90.00	90.00	120.0	B_1 (0.33333, 0.66667, 0.50000)
							B_2 (0.66667, 0.33333, 0.50000)

S2. Mechanical and thermodynamic stability for the bulk boron kagome lattice

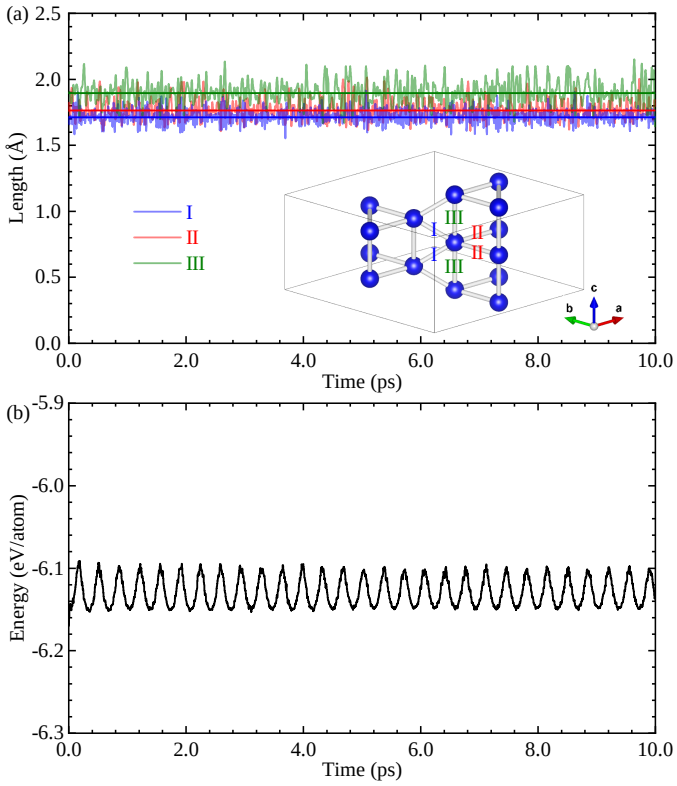

FIG. S2. Results of the molecular dynamics simulation at 300 K for the bulk boron kagome lattice. (a) Length evolution of three kinds of interatomic distances I, II, and III. The inset exhibits a $1 \times 1 \times 2$ supercell used to label the interatomic distances I, II, and III. (b) Helmholtz free energy evolution.

To see the mechanical stability, the elastic constants C_{ij} are calculated. For the hexagonal bulk boron kagome lattice, there are five independent elastic constants C_{11}, C_{12}, C_{13}, C_{33}, C_{44}, and $C_{66} = (C_{11} - C_{12})/2$. Our calculations show that $C_{11} = 286.2$ GPa, $C_{12} = 155.1$ GPa, $C_{13} = 51.4$ GPa, $C_{33} = 416.3$ GPa, $C_{44} = 72.2$ GPa, and $C_{66} = 65.6$ GPa. According to the mechanics criterion $C_{11} > |C_{12}|$, $2C_{13}^2 < C_{33}(C_{11} + C_{12})$, $C_{44} > 0$, and $2C_{16}^2 < C_{66}(C_{11} - C_{12})$ for hexagonal crystals in Ref. [1], we can easily figure out the bulk boron kagome is mechanically stable.

The thermal stability at finite temperature can be determined by molecular dynamics simulation. As an example, we perform a 10-ps *ab initio* molecular dynamics simulation within a $3 \times 3 \times 9$ supercell containing 486 atoms at 300 K for the bulk boron kagome lattice. The canonical ensemble is used, and the time step is set to be 2 fs. After simulation,

the atomic structure keeps intact without any lattice destruction, which suggests a good structural stability. Specifically, three types of interatomic distances nearby each boron atom keep small fluctuations around their balance lengths in the simulations, as shown in Fig. S2 (a), and the Helmholtz free energies also have small fluctuation around the balance value, as shown in Fig. S2 (b). Moreover, to test the effectiveness of the simulation, we also relax the supercell structures generated by molecular dynamics, and the intact ground-state configurations are obtained again, demonstrating that temperature induced atomic vibrations in our molecular dynamics simulation have not destroyed the atomic structure.

S3. Charge density and band-resolved Fermi surface for the bulk boron kagome

The charge density of the bulk boron kagome lattice is displayed in Fig. S3 (a). We clearly observe a zigzag-like distribution of electron cloud lying along the zigzag chains formed by the bonds I. We reveal that the bonds I are formed by the unbalanced sp^3 hybridization of s, p_x, p_y, and p_z orbitals but mainly from p_z electrons (about 60%) and s electrons (about 20%), referred to as σ' bonds. Compared with the sp-type σ bonds in δ_6 borophene [2], the bonds I here resemble, more or less, the sp hybridization of s and p_z orbitals but contain some p_x and p_y electrons due to the zigzag other than linear chains. At second level, a three-center bonding scheme gives rise to the bonds II that comprise s, p_x and p_y orbitals and thus the formation of in-plane triangular lattice, as shown in Fig. S3 (a), which is similar to the bonding mechanism in the flat triangular boron sheets [3], named as σ'' bonds. Finally, there is very low densities along the so-called "bonds" III, that is, the "bonds" III are not existent in the bulk boron kagome lattice although the length $d_{\mathrm{III}} = 1.892$ Å is small enough to form chemical bonds in pure boron systems. As a result, we can obtain the following picture of bonding: the zigzag-distributed bonds I and the in-plane three-center bonds II constitute the skeleton of bulk boron kagome lattice. Meanwhile, the length $d_{\mathrm{I}} = 1.707$ Å being shorter than $d_{\mathrm{II}} = 1.758$ Å signifies the stronger bonding of the bonds I relative to that of the bonds II.

In addition, the zigzag-like arrange of the bonds I combined with the absence of the so-called "bonds" III means a easily deformed quality along the zigzag direction (z direction), hinting a latent lattice instability (or charge density wave) on z direction, as demonstrated by the softening kink modes around the $\mathbf{q}_{\mathrm{s}}$ point in the main text.

Figure S3(b) exhibits the band-resolved Fermi surface with the projection of σ' orbitals for the bulk boron kagome, which indicates that the Fermi surface is formed by four bands crossing the Fermi level.

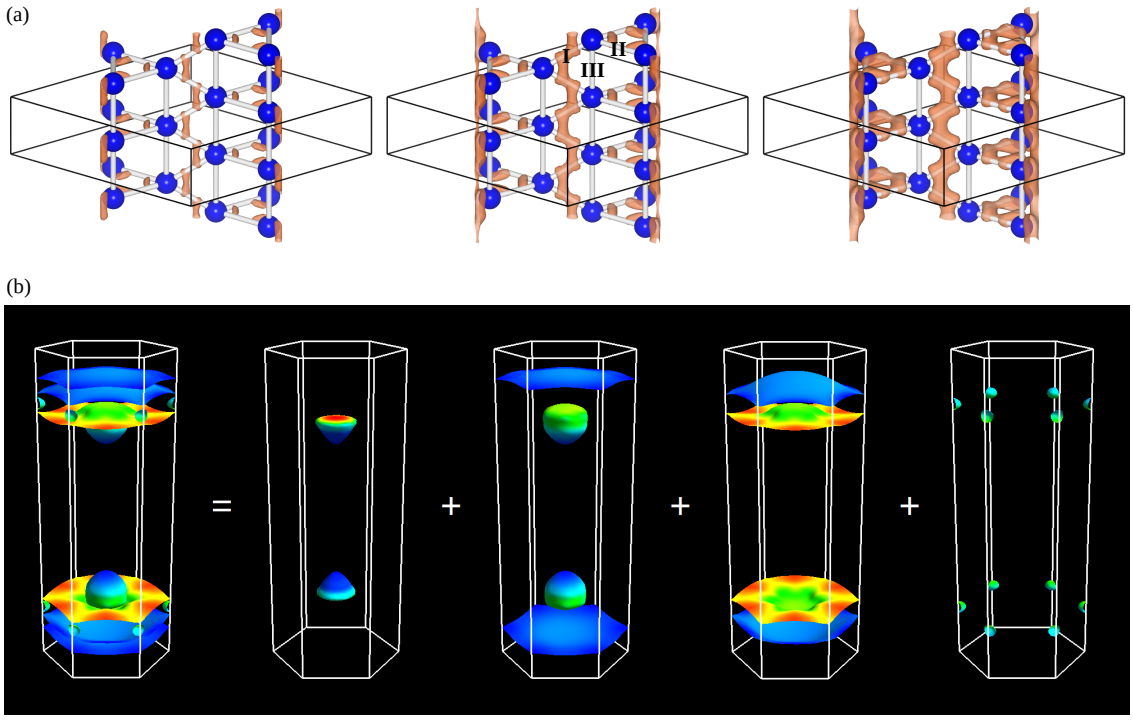

FIG. S3. (a) Charge density for the bulk boron kagome. From left to right, the orange contour represents the density of 0.87, 0.85, and 0.82 e/Å^3. (b) Band-resolved Fermi surface with the projection of σ' orbitals for the bulk boron kagome.

S4. Fermi surface with the projections of σ'' orbitals for the bulk boron kagome

The Fermi surface with the projections of σ'' orbitals for the bulk boron kagome is shown in Fig. S4. Unlike the σ'-orbital projected Fermi surface shown in Fig. 2(c) in the main text, the σ'' electrons distribute mainly on the regions away from the electronic wave vectors $\mathbf{k}_{\mathrm{F}} \approx 0.61 \times \Gamma\mathrm{A}$ on the Fermi surface. That is, the σ'' electrons have opposite distribution with that of the σ' electrons on the Fermi surface.

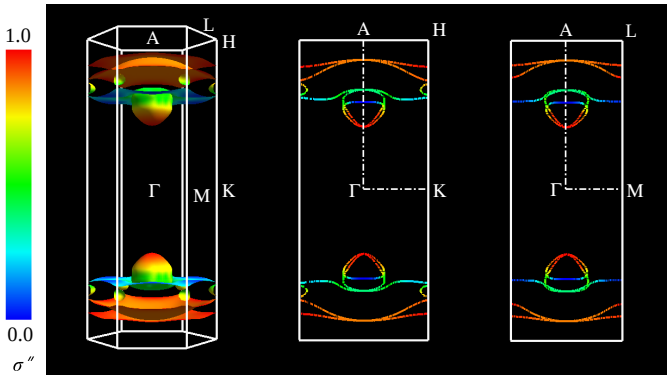

FIG. S4. Fermi surface with the projections of σ'' orbitals for the bulk boron kagome.

S5. Fermi surface nesting function $\zeta_{\mathbf{q}}$ for the bulk boron kagome

The calculated Fermi surface nesting functions $\zeta_{\mathbf{q}}$ in three typical surfaces of the whole BZ for the bulk boron kagome lattice are shown in Fig. S5(a). The corresponding results along high-symmetry lines of the BZ are plotted in Fig. S5(b), in which the electron-phonon coupling (EPC) parameters $\lambda_{\mathbf{q}}$ are also shown for comparison. From the definition of $\zeta_{\mathbf{q}}$ [4], the peaks of this function can be used for identifying nesting vectors which connect the parallel Fermi sheets of the Fermi surface (except $\mathbf{q} = 0$, where the peak is an artifactitious result of the definition). As shown in Fig. S5(a), the $\zeta_{\mathbf{q}}$ around the hexagonal cross section including ΓMK have relatively high values compared with those in other regions of the whole BZ, which can be explained by the rotational symmetry of the most regions of the Fermi surface on the ΓA axis and thus more feasible nesting of the states connected by the phonon wave vectors lying in the hexagonal plane with ΓMK. Remarkably, there is no clear indication of strong nesting effect in the whole BZ, especially at the $\mathbf{q}_{\mathrm{s}}$ point, as shown in Figs. S5(a) and S5(b), although the maximum EPC parameter $\lambda_{\mathbf{q}}$ is detected at the $\mathbf{q}_{\mathrm{s}}$ point. This finding rules out the nesting factor as a possible cause of strong EPC in the softening kink modes with wave vector $\mathbf{q}_{\mathrm{s}}$.

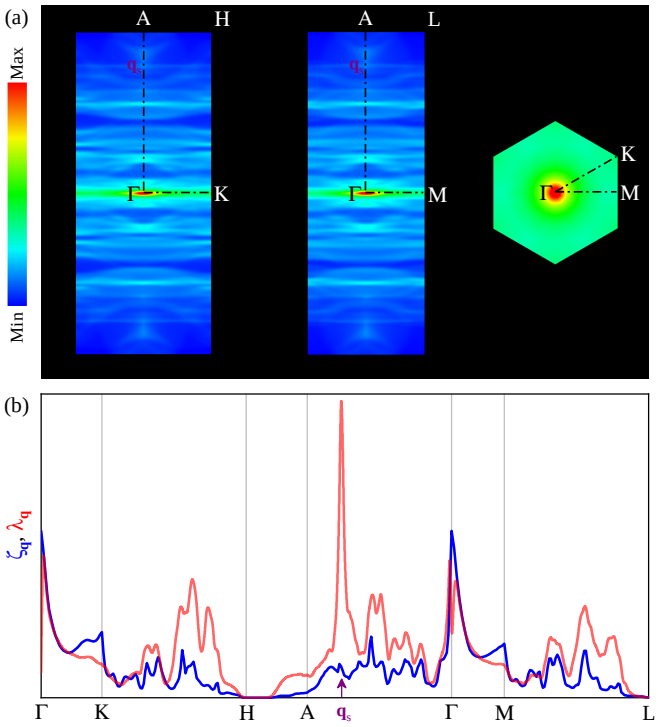

FIG. S5. (a) Fermi surface nesting functions $\zeta_{\mathbf{q}}$ in three typical surfaces of the Fermi surface for the bulk boron kagome. (b) Corresponding results along high-symmetry lines. The EPC parameters $\lambda_{\mathbf{q}}$ are also shown for comparison.

S6. Breaking of electronic degeneracies induced by the softest mode $\omega_s(q_c)$ at the point $\mathbf{q}_c = 0.8 \times \Gamma A$ for the bulk boron kagome

Except Fermi surface nesting effect, the breaking of electronic degeneracies by lattice fluctuations is another factor to cause strong EPC in the softening kink modes. To check this factor, we focus on the softest mode $\omega_s(q_c)$ at the phonon wave vector $\mathbf{q}_c = 0.8 \times \Gamma A \approx \mathbf{q}_s$, as shown in Fig. 3(a) in the main text. However, the polarization vectors of the modes at $\mathbf{q}_c$ are described by complex numbers. To gain real values of the polarization vectors, a $1 \times 1 \times 5$ supercell of the bulk boron kagome is created to fold the $\mathbf{q}_c$ point into the BZ center, and then the vibrational properties of the created supercell are calculated. Based on the folding principle and phonon energy difference, on can easily infer that the optical mode E″ at the Γ point in the $1 \times 1 \times 5$ supercell, as shown in Fig. S6, is actually the softest mode $\omega_s(q_c)$ at the $\mathbf{q}_c$ point in the primitive cell. As shown in Fig. S6, this E″ mode can induce conspicuous atom displacements along zigzag direction (z direction), which easily drives the

stretching of the *sp*-like I-type bonds in the system.

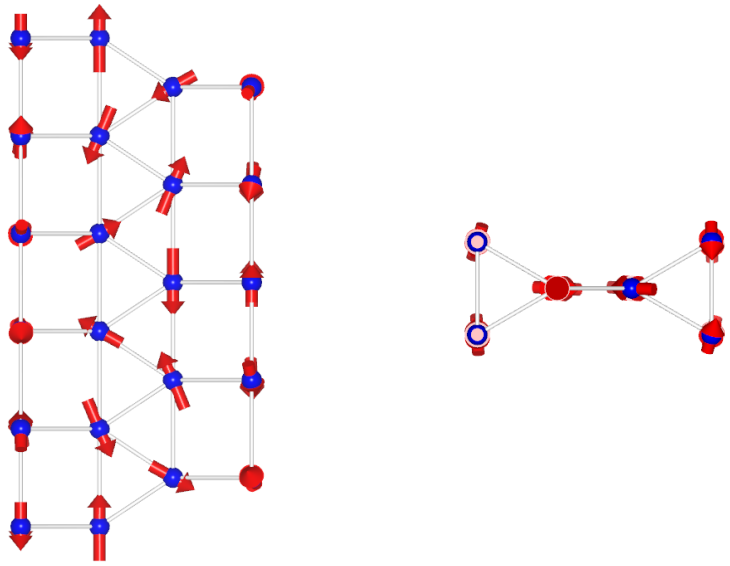

FIG. S6. Lateral and top views of the optical mode E″ for the $1 \times 1 \times 5$ bulk boron kagome.

To investigate the breaking of electronic degeneracies by the lattice fluctuations related to the E″ mode and the consequent removal of electronic weight from the electronic density of states (EDOS), the required atom displacements induced by the E″ mode are determined by

$$\Delta\tau_{\kappa,\alpha}(x) = \sqrt{\frac{M_0}{M_\kappa}} e_{\kappa,\alpha} x, \tag{1}$$

where M_κ is the nuclear mass of atom κ and M_0 is the proton mass. From the vibrational properties at the Γ point in the $1 \times 1 \times 5$ supercell, the real polarization vectors $e_{\kappa,\alpha}$ of the E″ mode can be obtained. Then the atom displacements related to a parameter x can be easily calculated from equation (1). Here we select the atom displacements correspond to the case with $x = 1$ Å. Through adding these atom displacements into the optimized $1 \times 1 \times 5$ supercell, the required configuration with the influence of the E″ mode is created. At last, the band structure and EDOS for the $1 \times 1 \times 5$ configuration with these added atom displacements are calculated, as shown in Fig. 3(d) in the main text, in which the band structure is unfolded into the BZ of the primitive cell.

Obviously, after considering the influence of the E″ mode, the bands with sp_z orbitals close to the Fermi level generate some avoided crossings, especially on the high-symmetry

lines ΓA, ML, and KH, as shown in Fig. 3(d) in the main text, which demonstrates the breaking of electronic degeneracies by the lattice fluctuations related to the E″ mode that can induce the stretching of the σ-like I-type bonds. As a result, the EDOS of sp_z states around the Fermi level is evidently declined relative to that of undistorted structure, and thus the decline of total EDOS, demonstrating the removal of electronic weight from the EDOS close to the Fermi level.

S7. Mode-resolved isotropic Eliashberg spectral function $\alpha^2F(\omega)$ with the cumulative EPC strength $\lambda(\omega)$ for each phonon branch of the bulk boron kagome

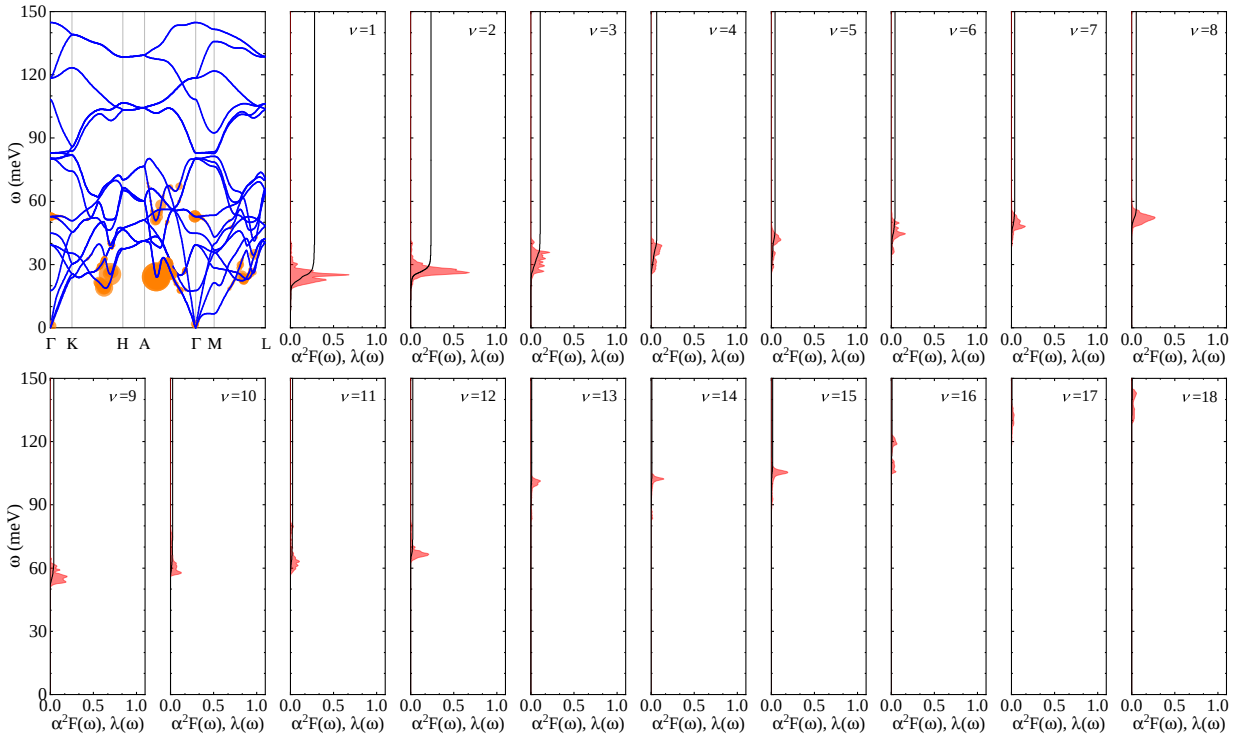

FIG. S7. Phonon dispersion and mode-resolved isotropic Eliashberg spectral function $\alpha^2F(\omega)$ with the cumulative EPC strength $\lambda(\omega) = 2\int_0^\omega \alpha^2F(\omega')/\omega' d\omega'$ for each phonon branch of the bulk boron kagome.

* ligeng@nscc-tj.cn

† y.zhao@ytu.edu.cn

[1] F. Mouhat and F.-X. Coudert, Necessary and sufficient elastic stability conditions in various crystal systems, Phys. Rev. B **90**, 224104 (2014).

[2] J. Kunstmann and A. Quandt, Broad boron sheets and boron nanotubes: An ab initio study of structural, electronic, and mechanical properties, Phys. Rev. B **74**, 035413 (2006).

[3] H. Tang and S. Ismail-Beigi, Novel Precursors for Boron Nanotubes: The Competition of Two-Center and Three-Center Bonding in Boron Sheets, Phys. Rev. Lett. **99**, 115501 (2007).

[4] S. Poncé, E. Margine, C. Verdi, and F. Giustino, EPW: Electron–phonon coupling, transport and superconducting properties using maximally localized Wannier functions, Comput. Phys. Commun. **209**, 116 (2016).